



Space debris generation in GEO: Space materials testing and evaluation

S. Duzellier^a, P. Gordo^b, R. Melicio^{c,d,*}, D. Valério^c, M. Millinger^e, A. Amorim^b

^a ONERA/DPHY, University of Toulouse, France

^b CENTRA, Faculdade de Ciências da Universidade de Lisboa, Lisboa, Portugal

^c IDMEC, Instituto Superior Técnico, Universidade de Lisboa, Portugal

^d ICT, Universidade de Évora, Portugal

^e ESA/ESTEC, European Space Agency, Netherlands

ARTICLE INFO

Keywords:

Space debris
Space materials
Geostationary orbit
Geostationary transfer orbit
Spacecrafts
Space environment

ABSTRACT

The aim of this work is to evaluate what happens to the spacecraft materials beyond the spacecraft End of Life. A review of spacecraft external materials and effects of space environment is presented. This paper results from a continued study on spacecraft material degradation, and space debris formation in geostationary orbit (GEO). In this paper a 20-year GEO dose profile that combines simultaneous UV, particles irradiation and thermal cycling was applied to a set of external spacecraft materials. These materials comprised MLI assemblies, Velcros fixation and spacecraft painting. The evaluation of these external spacecraft materials, exposed to simulated space environment have confirmed the criticality of degradation of MLI, Velcros fixation and painting, with delamination mechanisms and particulate contamination. The synergy of space radiation (particles, UV) and thermal cycling ages the material and induces mechanical stress, causing creation of brittle surfaces, cracks and delamination. These phenomena cause serious damage to exposed surfaces, changing the surfaces thermo-optical properties, and may induce the generation of space debris. In particular, experimental results show the delamination of internal MLI layers and the severe degradation of the Velcros.

1. Introduction

Since the first man-made satellite launched in 1957 by Soviet Union, space activities have become more and more intensive. Human space exploration activity in the near-Earth space (LEO and GEO) has left behind a tremendous number of debris that poses a potentially significant danger to active satellites, spacecraft and people working in extravehicular activity [1–4]. The number of space debris in orbit, consisting of bodies of disparate sizes, has increased. Examples of such debris are decommissioned satellites, rocket bodies (e.g. rocket upper stages, adapter rings), spacecraft external materials as paint flakes, payload shrouds, explosive bolts remains, instrument covers, slag particles [5,6] (see Fig. 20).

Potential colonization of Mars and the Moon puts an additional pressure on how we manage the near-Earth space, since in the future we may need this space to deploy long-living bases and transition hubs to facilitate growing traffic from the Earth to extra-terrestrial outposts (see Fig. 19).

In this paper we address the formation of space debris and the factors

that cause them, in particular for multilayer insulation materials, in particular when employed in a geostationary orbit (GEO). The main contributions are: (i) A review on spacecraft materials and effects of space environment on the materials; (ii) Description of the testing implementation for a high dose profile that simulate a 20 year GEO mission; (iii) Evaluation of radiation effects on the materials (mechanical properties and TO); (iv) identification of severe degradation of MLI internal layers and MLI Velcros; (iv) Size distribution of debris for the degraded MLI layers.

The paper is structured as follows: Section 2 introduces the previous research on the system. Section 3 explains the experimental methods. Section 4 presents the experimental results. Finally, Section 5 outlines conclusions.

2. State of the art

Today, space debris has become a huge concern for orbital missions that makes remediation a critical and necessary action [7]. The spatial density of space debris is often used to define the number of resident space objects (RSO) per unit volume as function of the altitude [8] as

* Corresponding author. IDMEC, Instituto Superior Técnico, Universidade de Lisboa, Av. Rovisco Pais, 11049-001 Lisboa, Portugal. Tel.: +351 218 417 351.

E-mail addresses: sophie.duzellier@onera.fr (S. Duzellier), prgordo@fc.ul.pt (P. Gordo), ruimelicio@gmail.com (R. Melicio), duarte.valerio@tecnico.ulisboa.pt (D. Valério), Mark.Millinger@esa.int (M. Millinger), aamorim@sim.ul.pt (A. Amorim).

<https://doi.org/10.1016/j.actaastro.2021.12.036>

Received 26 September 2021; Received in revised form 19 December 2021; Accepted 21 December 2021

Available online 24 December 2021

0094-5765/© 2021 IAA. Published by Elsevier Ltd. All rights reserved.

Nomenclature

Acronyms

AO	Atomic oxygen
CVCM	Collected volatile condensable material
ESD	Electrostatic discharge
ESH	Equivalent sun hours
EO	Earth observation
FSR	Flexible solar reflector
GEO	Geostationary orbit
LEO	Low Earth orbit
MLI	Multilayer insulation

OSR	Optical solar reflector
PSA	Pressure sensitive adhesive tape
LEO	Low Earth orbit
RML	Recovered mass loss
RSR	Rigid solar reflector
SC	Solar constant
SSM	Second surface mirrors
TC	Thermal cycling
TML	Total mass loss
TO	Thermo-optical
VUV	Vacuum ultra-violet
X-ETFE	Ethylene-tetrafluoroethylene

shown in Fig. 1.

Fig. 1 shows that the spatial density is higher in Low Earth orbit (LEO) and geostationary orbit (GEO). It can also be observed that the spatial density is slightly higher in GEO regime than it is in LEO. Note that RSO spatial density depends also on orbit altitude and declination. GEO spacecrafts or satellites are exposed to the outer radiation belts, solar flares and cosmic rays. Spacecrafts in GEO orbits are near the magnetopause, hence they are susceptible to high energetic plasmas during geomagnetic sub storms (in the tail of magnetosphere) [9].

In previous research we have reported a study on generation of space debris in simulated LEO conditions [10,11]. Also, we have reported a first incite on a study on generation of space debris in simulated GEO conditions [12].

Spacecraft external materials play an important factor in satellite protection from space environment. In the past there have been cases of satellites failures due to the satellite external material degradations and respective change in thermo-optical properties. Midori – II, an Earth observation (EO) satellite, has stopped working in 2003 possibly due to X-ETFE degradation (change in the thermo-optical properties) due to UV [13]. It has been recognized that external spacecraft material studies play an important role in satellite reliability. However the vast majority of previous studies are focused in material degradation in space environment, leaving debris generation less studied.

One contributor to space debris generation is the degradation of external spacecraft materials exposed to space environment. As a summary, depending on the environment and the type of family of materials, the main degradation mechanisms that can be observed are:

- Temperature: mechanical stress due to thermal cycling (TC), higher scission/x-linking ratio or colour centres bleaching at temperature higher than room temperature (RT);
- UV (affect mostly polymers): bonds breaking and rearrangement (photolysis), excitation and ionization;
- Charged particles: ionization (bonds breaking, radicals and colour centres depending on material type), displacement damage (radiolysis), physical sputtering (solar wind), blistering (metals only, and for large fluency);
- Atomic Oxygen (AO) affects polymers, metals, thin coatings: oxidation leading to erosion of surface materials.

With operational conditions combining these constraints, synergy will lead to enhanced degradation and potential generation of debris. In this problematic, surface (thermo-optics parameters) and mechanical properties are of prime importance.

In GEO, the synergy of space radiation, i.e. electrons, protons, UV and thermal constraints is considered as main contributor to the degradation-induced debris process with the following mechanisms:

- An enhanced degradation of thermo-optical properties (increased absorptance) will result in material temperature increase which in turn will impact on mechanical stress level;
- The oxidation of surface and change in surface state may result in more brittleness that can jeopardize the integrity of the material (coating or films) via self-debris generation or impact-induced;
- Enhanced degradation at stress location stress (e.g. multilayer insulation (MLI) fixation point, coating/substrate interfaces).

2.1. Degradation factors and experimental constrains

To evacuate the materials for space applications it is usual to perform a series of qualification tests; however, the implementation of this test is subject to experimental constrains reported in this section:

- Air vacuum testing considerations

The presence of oxygen during irradiation induces a mechanism of oxidation reactions and the formation of free radicals in the material. This mechanism impacts the scission/cross-linking rate of the materials. It can be observed an increase, of several orders of magnitude, of polymer degradations, between radiation response in air (worst case) and under vacuum.

Annealing mechanisms are also affected by oxygen during vacuum-to-air transitions with kinetics varying from minutes to hours [14,15].

Ground testing of surface materials (particles exposures) requires vacuum conditions ($<10^{-7}$ mbar), so that contamination of surfaces is avoided.

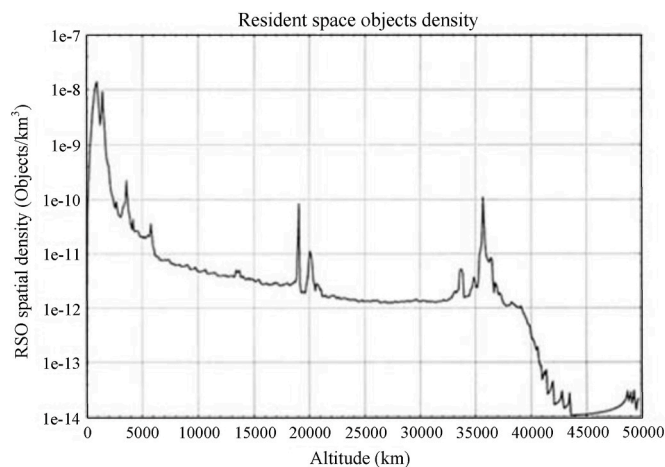


Fig. 1. Resident Space Objects density.

- Temperature

Temperature is a major parameter in the process of material degradation when acting in synergy with other components of space environment, especially radiation.

For organic materials, degradation increases with temperature due to greater chain mobility (higher scission/x-linking ratio) [15]. In inorganic materials, temperature governs annealing of coloured centres as observed in optics [16].

At low temperature, synergy with space radiation is not straightforward and depends on material type [17,18]: degradation mechanisms are “frozen” in materials sensitive at room temperature while no significant change is observed in more resistant materials (epoxy, polyimide); silicones are more sensitive at low temperatures.

For missions with strong temperature constraints (range and cycling), it was shown that the representative simulation of the mission profile was required to include a reliable estimate of materials degradation and prediction of End-of-Life performances [19].

Moreover, at macroscopic level, temperature cycling (alone or in synergy with space radiation) induces mechanical stress that can result in enhanced degradation either overall or at stress location [20,21].

The temperature range for ground simulation (i.e. material testing) is usually larger than operational conditions, but the number of cycles is usually lower. The higher temperature range can be considered an accelerated degradation mechanism.

- Particle dose rate, UV flux on ground simulation (i.e. radiation exposure acceleration impact)

Particles and UV acceleration at ground facilities are strongly different due to different technical limitations. Acceleration may induce abnormal dose rate effects in materials. When particles irradiation takes place in air, dose rate effects have been observed (the lower the dose rate, the higher the oxidation rate).

In vacuum, some cases of dose rate effect have been observed, affecting measurements on volatile products emission, but the impact on material properties at macroscopic level is not significant [22]. White paints with the higher acceleration are the worst-case condition [23].

Dose rate effects with charged particles are very material-dependent and may be associated with parasitic mechanisms, such as over-heating of samples. Sample over heating due to large flux may lead to recovery effects that are not representative of orbit conditions (underestimate of degradation).

Regarding UV/VUV, only few papers in the literature report on acceleration effect on material response and degradation [24–26], and this over a limited range of solar constant (SC). Most of the existing solar or UV simulator provides acceleration factors in the 2–15 SC range. UV acceleration is usually limited, as the light absorption in the exposed material creates a temperature increase leading to thermal effects. That is the reason why norms and standards define a maximum UV acceleration [27–29].

Regarding VUV, high acceleration can be obtained (in the 115 nm–180 nm range) with deuterium lamps for instance. VUV only affects surface properties.

Note that, from the debris generation standpoint, UV acceleration does not seem to be much relevant (unless participating to the sample temperature local or global increase); the total Equivalent sun hours (ESH) seen by the sample (total dose) are on the other hand very relevant.

- GEO particles dose profile

The radiation dose on materials drops rapidly with depth. So, representativeness of dose profile is a critical parameter from the thermo-optic properties and for coating adhesion (i.e. dose at coating/substrate interface).

In orbital conditions, surface dose is deposited by VUV/UV, protons with energy lower than 0.5 MeV and electrons with energy lower than 100 keV. At ONERA, the typical GEO dose profile is simulated as disclosed in Fig. 2 (with 2 proton beams and 1 electron beam).

In Fig. 2 GEO is the total cumulative dose in a one-year GEO orbit, calculated by ONERA. The electromagnetic radiation only affects surface properties, as wavelength and attenuation length of most (opaque) materials leads to dose deposition in the first microns (or less) [30] as shown in Fig. 3.

It is usually recommended to use Xenon lamps which provide representative solar spectrum and to filter the >400 nm range to avoid overheating of samples.

Dose equivalence can be applied between Xenon, Xenon–Mercury, and Mercury lamps integrating irradiance over the 200 nm–400 nm range. This equivalence is considered valid if the threshold energy for degradation is known [29].

- Material degradation mechanisms and debris generation

In MLI, fragments release is assumed to be described by a three-stage process: 1) Tear initiation in regions of highest stress and enhanced by material degradation (UV, AO or particle dose); 2) Tear propagation; 3) Foil separation.

In a simulation environment, using a representative dose profile, tear initiation can be reproduced on the 1st MLI layer, while the inner layer receives a lower dose than the one expected from the dose profile (otherwise inner layers would be over tested compared to the external). The implementation of a constant dose over the whole assembly set by surface dose (very strong in GEO) is technically difficult as it requires very large electron fluency (and thus an unrealistic long irradiation).

For paints, two mechanisms of debris generation can be considered: 1) ageing processes leading to the creation of a brittle surface layer, which may crack and lead to the generation of spalling off; 2) large temperature fluctuations leading to a thermal expansion of coatings and substrates at different rates. The creation and growth of cracks, caused by local thermal stress combined with AO, UV or particle dose, leads to the delamination of the coating layer.

In a simulated environment, a representative dose profile allows the reproducing of delamination mechanisms, at interface (actual dose at coating/substrate interface) and defect locations (actual surface dose).

- Combined/sequential testing (particles, UV)

Combined testing is justified in presence of synergy between different constraints. Simultaneous exposure of materials to particles

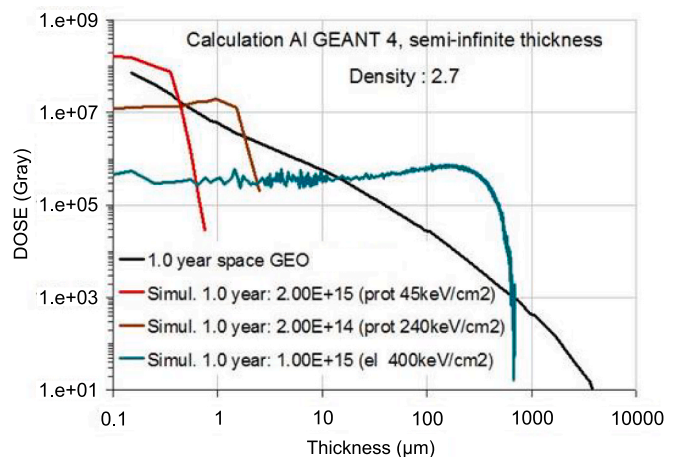


Fig. 2. Typical GEO dose profile at SEMIRAMIS facility simulated with 2 proton beams and 1 electron beam (fluence for 1 year mission).

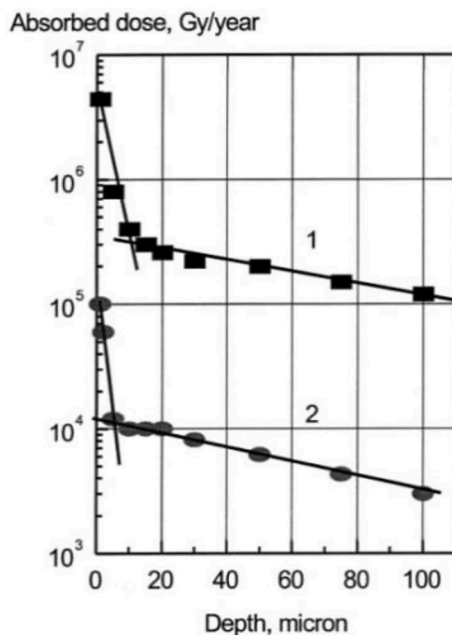


Fig. 3. Dose profile in GEO for 2 materials (1- Kapton in GEO, inclination $0 \pm 160^\circ$ Western longitude, 2- cerium glass in polar orbit 800 km).

- Solar simulation

and temperature and then to UV and temperature is commonly performed. Simultaneous exposure with different types or energies of particles (electrons and protons) is technically more difficult as it depends on the facility construction (capability to operate several accelerators or electron/proton guns at the same time).

Moreover, even if simultaneous exposure to particle and UV is feasible, acceleration factors are very different (traditionally >1000 for particles flux, on the order of 10 with UV flux) leading to irradiation times much longer with UV.

Typically, simulating a 15-year GEO dose with particles takes 3 weeks of machine time, whereas only 8-year GEO UV ESH will be reached after more than 2 months exposure with standard acceleration. However, long-term testing of surface materials has shown UV-induced degradation saturation, that allows limiting UV exposure to a reasonable time.

A sequential exposure approach can also be used. In this approach, materials are exposed to particles (protons, electrons) and UV in successive steps. It allows for monitoring separate degradation induced by each environmental component.

Few data exist comparing sequential versus simultaneous approaches [19,31] but some difference can be expected due to the presence of UV- or electrons-induced annealing phenomena. That is why, in a sequential approach, the sequence order is important [31].

Debris generation by self-flaking requires a large accumulated dose (up to 15 years–20 years GEO). Acceleration is limited with UV, therefore simultaneous UV/particles exposure is preferred to optimize testing duration. Moreover, representativeness is ensured by simultaneous exposure, and UV also contributes to thermal stress applied during irradiation.

For the same reasons and for the sake of representativeness, the temperature constraint (usually constant level) is applied in synergy with the other environmental conditions. However, thermal cycling requires specific capabilities; therefore, TC is usually applied before or sometimes after ageing [20,32,33]. Sequential mode can therefore be used for qualitatively simulating degradation mechanisms; nevertheless, the simultaneous mode is preferred for quantitative measuring degradation levels [19].

Ageing test facilities are not designed for thermal vacuum testing, and, depending on capabilities (temperature range and number of cycling), TC could be partly applied during ageing optimizing test duration.

2.2. Degradation of materials and failure mechanisms

Charged particles (trapped electrons and protons, solar event protons — x-rays on the side facing sun — and solar wind) are at the origin of the ionizing dose profile absorbed by the materials. Surface materials, as MLI and paints, are not shielded and therefore are subject to a worst-case environment for a given mission with important dose surface (>109 krad). Because of the energy spectra and mode of interaction of particles with matter, protons are responsible of surface dose (first μm) and electrons of bulk dose. The dose in rad/year and for different orbits is presented in Table 1.

For orbits that cross trapped belts in GEO, the absorbed dose profile exhibits a strong variation with depth as protons are stopped at the very surface ($<2 \mu\text{m}$). The dose profile in GEO for 2 materials (1- Kapton in GEO orbit inclination $0 \pm 160^\circ$ Western longitude, 2- cerium glass polar orbit 800 km) [34] is shown in Fig. 3.

In ionization process, an atom loses an electron and forms an ion (whatever the chemical link at play). At material level (organic), these excitation/ionization mechanisms will result in the formation of free radicals or ions. These reactive intermediates are capable of initiating chemical reactions which result in scission as well as in cross-linking reactions. The macroscopic effects are then linked to the accumulation with time of the ionizing dose (namely “cumulated effect”) inducing surface and volume phenomena.

The same particles are also at the origin of displacement dose (non-ionizing) leading to creation of interstitials-vacancies, single or cluster of defects. The macroscopic effect of such phenomena mostly concerns inorganic materials and large fluence.

UV is critical for surface materials facing the sun (AM0 solar spectrum, ASTM490) but also facing earth due to the albedo effect (about 30% AM0 in terms of received energy). AM0 solar spectrum is a standard solar spectrum used for space applications, i.e. solar spectrum without atmosphere.

The UV radiation spectrum comprises wavelengths of between 200 nm and 400 nm, which correspond to energies of between 600 kJ/mol and 300 kJ/mol. These energies are in the same range as the bond energies of many organic compounds. Chemical reactions are induced when specific functional groups absorb the UV radiation. Free radicals liberated in the excitation/ionization process will trigger further reactions (bonds breaking and rearrangement: photolysis). Signs of photo-degradation include embrittlement (surface cracking), discolouration and loss of transparency.

2.3. External spacecraft materials

The typical external spacecraft materials are listed in Table 2.

One of the main tasks of paints is to support spacecraft thermal control, by the reflection or absorption of electromagnetic radiation from the sun and by radiative emission to space.

Spacecraft passive thermal design allows thermal energy channels along the exterior, so that appropriate temperatures are maintained in the various elements of the spacecraft. Also, another important aspect of

Table 1
Dose in rad/year and for different orbits.

Depth	0.2 μm	2 μm	20 μm
LEO			2×10^5
HEO			1.2×10^6
GEO	1×10^{10}	3×10^8	1×10^8
Lagrange L1 & L2	3×10^8	6×10^6	6×10^5

Table 2
Typical external spacecraft materials.
• Paints

Product type	Sub-categories	Description	Materials examples	Examples of applications
Thermal control paints	- White paint - Black paints - High temperature paints	Spacecraft thermal control, by optimizing the spacecraft exterior surfaces thermo-optical specifications. Applied to control the absorption and emission of energy on exposed spacecraft surfaces.	- NASDA white paint (NASDA-1049/101-S), - NOVA astro white, - S13GP L0-1,	- White ceramic thermal insulating coatings for BepiColombo. - Spacecraft exterior protection (radiation, UV and AO). - Black paints can be used in heat shields for micro and nanosatellites to protect satellites when being transferred from orbit.
Optical solar reflector (OSR)	- OSR - Rigid solar reflector (RSR) - Flexible solar reflector (FSR) - Second surface mirrors (SSM)	Flexible optical solar reflectors (OSRs) are used as satellite radiators. They have low absorption and high IR emissivity. The top layer of OSRs can be made of silica over a metallic reflective layer. The silica material has a high IR emission coefficient and low absorption.	- FSR - multi-layered film ITO/CeO2/polyetherimide/Ag/Ni alloy - IT O/CeO/polyetherimide/Ag/Ni	- Thermal control coating. - Outer skin of spacecraft and launch vehicles.
ATOX protection coatings	NA	Protection from atomic oxygen. Can be applied on top of electronics as protective coating.	MAPATOX K, MAPATOX 41B, silicon paints, ceramer paints (part ceramic part polymer)	Protection from ATOX.
Thermal control foil	NA	Single polymeric foil with a metallic coating.	Aluminium coated Mylar™, Teonex™, UPILEX, Colourless polyimide	Parabolic antennas, solar wings, and thermal control systems.
Thermal control blanket (i.e. MLI)	NA	Its purpose is to thermal isolate the satellite, acting as radiation barrier and decreasing heat losses. Stack of thin polymeric layer (5–25 foils), separated by spacer or mesh or embossed, crinkled, external and innermost layers differ from the inner ones.	Aluminised-Teflon (Al-FEP) Polyimide (PI) films (e.g. Kapton), Mylar™	Hubble space telescope thermal shields.
Adhesives	NA	Structural gluing of satellite parts.	DC 93–500, RTV-5690	Solar cell adhesive, encapsulate, potting.

the paint is its electrically conductivity, forming a protection against the formation of electrostatic charges, and the resulting discharges (ESD).

Space environment conditions that most degrade paints are UV radiation, AO, particle radiation (electrons and protons), and thermal cycles. The dose profile, number of cycles, temperature limits, strongly depend on the spacecraft attitude and orbit during the mission.

The paint degradation by space environment will have a strong impact in the function of paint (i.e. TO properties).

Regarding paints applications, one can classify the paints by the following subclasses:

- White paint. These paints typically have low absorptance and high emissivity. White paints are used in the spacecraft exteriors to decrease temperature (e.g. to paint spacecraft radiators).
- Black paints. These paints typically have high absorptance and high emissivity. Black paints are mainly used in the interior of satellites, though also found in the exterior of spacecraft (e.g. in optical spacecraft parts to decrease stray light propagation).
- High temperatures paint. These paints protect spacecraft from high temperatures, e.g. when re-entering the atmosphere.

Table 3
Lists of some of the current space grade paints.
• MLI materials

Manufacturer	Product	Base Composition	Colour	Absorptance	Emittance	Outgassing
Lord Corporation	Chemglaze H32	Polyurethane	Matt-black	0.95	0.85	TML = 1.6%, RML = 0.9%, CVCM = 0.04%
Lord Corporation	Chemglaze L300	Polyurethane	Matt-black	0.955	0.85	TML = 1.7%, RML = 0.9%, CVCM = 0.04%
Lord Corporation	Chemglaze Z306	Polyurethane	Black	0.95	0.9	TML = 1.5%, RML = 0.6%, CVCM = 0.03%
Acheson Colloiden	Electrodag 501	Fluorinated binder	Black	0.965	0.829	TML = 0.86%, RML = 0.44%, CVCM = 0.00%
Acheson Colloiden	Electrodag 503	Fluorocarbon binder	Silver	0.37	0.44	TML = 0.22%, RML = 0.21%, CVCM = 0.06%
Société MAP S.A.	PCBZ	Silicone/Metallic	Matt-White	0.2 ± 0.04	0.83	TML = 0.55%, RML = 0.52%, CVCM = 0.08%
Société MAP S.A.	PCBE	Silicone	Matt-White	0.25–0.29	0.88	TML = 1.15%, RML = 0.44%, CVCM = 0.03%
Société MAP S.A.	PSB	Potassium Silicate	Matt-White	0.14 ± 0.02	0.88	TML = 3.04%, RML = 0.04%, CVCM = 0.00%
Société MAP S.A.	PSBN	Silicate	Matt-White	0.15 ± 0.02	0.92 ± 0.02	RML = 0.29%, CVCM = 0.00%
Société MAP S.A.	MAP – PU1	Polyurethane	Matt-black	0.96 ± 0.02	0.89	RML = 0.56%, CVCM = 0.09%
Société MAP S.A.	PNC	Silicone	Matt-black	0.98 ± 0.02	0.91 ± 0.03	TML = 0.91%, RML = 0.52%, CVCM = 0.00%
Société MAP S.A.	MAP – PUC	Polyurethane	Black	0.94 ± 0.02	0.8	TML = 0.83%, RML = 0.55%, CVCM = 0.02%
Société MAP S.A.	MAP – SG120FD	Silicone	Matt-White	0.17 ± 0.04	0.87 ± 0.02	TML = 0.55%, RML = 0.54%, CVCM = 0.04%
Société MAP S.A.	SG121FD	Silicone	Matt-White	0.17 ± 0.02	0.88 ± 0.03	TML = 1.30%, RML = 0.28%, CVCM = 0.08%
Société MAP S.A.	SG122FD	Silicone	Matt-White	0.18 ± 0.02	0.90 ± 0.03	RML = 0.74%, CVCM = 0.07%
Société MAP S.A.	SCK5	silicone	Matt-White	0.29 ± 0.02	0.89 ± 0.04	–
Société MAP S.A.	PUK	Polyurethane	Matt-black	0.97 ± 0.02	0.91 ± 0.03	RML = 0.56%, CVCM = 0.00%
Akzo Nobel Aerospace Coatings	PSG 120 FD	Silicone	White	0.19	0.88	TML = 0.56%, RML = 0.54%, CVCM = 0.03%
ALION	Z93P	Silicate	White	–	–	–
Previous IITRI (USA)						
ALION	SG13GP6N	Silicone	White			
Previous IITRI (USA)						

- Other paints (e.g. metal paints). These include metal plating of gold, silver or even copper, helping to protect internal electronics by reflecting UV and infrared radiation [35].

The list of some of the current space grade paints is presented in Table 3.

Multilayer insulation (MLI) material provides high performance and specifically addresses all modes of heat transfer through the basic design of the system. For ground applications MLI is often used inside of a vacuum chamber, eliminating gas convection, and minimizing gas conduction to the molecular scale. Reflective shields are used to minimize radiation heat transfer inversely proportional to the number of shields. Low conductivity spacers are used to prevent the metallic based reflective shields from touching; they also minimize the conduction through the blanket itself. Much care is taken to design the MLI blanket such that it minimizes heat transfer in every manner including edges, seams, and installation procedure.

The environmental effects that cause degradation of the MLI are primarily temperature cycling, solar radiation, particle radiation, and AO. Although VUV, from solar radiation, is abundantly present at all altitudes, AO is particularly a problem in LEO. The MLIs are made from polymer films; the AO reacts with the organic species and erodes the polymer. This phenomenon is known as AO erosion and is measured in mass loss.

The key MLI specifications and material characteristics that are correlated with the MLI materials degradation, and therefore also correlated to debris generation, are TO properties; MLI stack configuration in terms of number, thicknesses, and materials of the layers; operational temperatures.

- MLI application methods

Regarding MLI fixation methods, the most common fixation methods are:

- 1) Stand-offs/clipwasher fixation with the stand-offs bonded or screwed to the structure. This method is considered the most reliable fixation method. Stand-offs is available in different dimensions and can be custom made to the specific application.
- 2) Velcro fixation: Velcro stapled to blanket, and counterpart glued to structure using pressure sensitive adhesive tape (PSA) or adhesive.
- 3) Bonding of the blanket directly to structure by means of pressure-sensitive adhesive tape (PSA).

An example of MLI application is shown in Fig. 4.

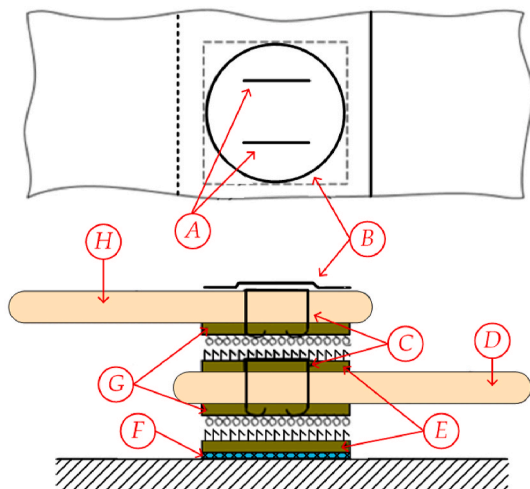


Fig. 4. Example of MLI application with velcro.

In Fig. 4 (A) are the staples; (B) is the cover tape; (C) are the staples; (D) the blanket #2; (E) is the Velcro type 2; (F) is the adhesive; (G) is the Velcro type 1; (H) is the blanket #1.

3. Experimental methods

A simulation of a 20-year of GEO dose profile was performed at ONERA, DESP, Department of Space Environment, France. The simulation combines particles and UV doses in synergy with thermal cycling to investigate potential generation of debris from the ageing of surface materials.

3.1. Tested materials and mounting on sample plate

- MLI test samples

Two MLI layouts strips of 44 mm × 120 mm were prepared for the GEO test campaign: one MLI layout with an outer layer of black Kapton (used in satellites with optical instruments), and another layout with an outer layer of Kapton. The MLI layouts materials are depicted in in Fig. 5.

In Fig. 5 (a): (A) is 1 × 1 mm of Kapton; (B) is VDA coating; (C) is 5 × Dacron spacer plate; (D) is 5 × 0.3 mm Kapton perf.; (E) is 5 × Polyester Fleece Spacer PV-8g; (F) is 5 × 0.25 mm Mylar perf.; (G) is 1 × Polyester Fleece Spacer PV-8g; (H) is 1 × 1 mm Mylar foils. In Fig. 5 (b): (I) is 1 × 1 mm of black Kapton XC; (B) is VDA coating; (C) is 5 × Dacron spacer plate; (D) is 5 × 0.3 mm Kapton perf.; (E) is 5 × Polyester Fleece Spacer PV-8g; (F) is 5 × 0.25 mm Mylar perf.; (G) is 1 × Polyester Fleece Spacer PV-8g; (H) is 1 × 1 mm Mylar foils.

Two different fixation methods were implemented for each MLI strip. The MLI strips were grounded during the test. The fixations were: Velcros (ref SJ3571 Nylon6.6, loops part only) attached with staples; and Stand-off with clip/washers in Vestel.

The implementation of the MLIs in the sample holder is depicted in Fig. 6.

- Paints test samples

The selected paints are used in satellites' exteriors; different substrates and base compositions were considered. The tested paints (procured at MAP), with dimensions 19.8 mm × 19.8 mm, are presented in Table 4.

SG121FD is white silicone paint and is a frequently used paint in satellites. PSB is white silicate paint; it was applied on two different substrates (AUG4 and CFRP). PNC is black silicone paint and is used in satellites that have optical instruments.

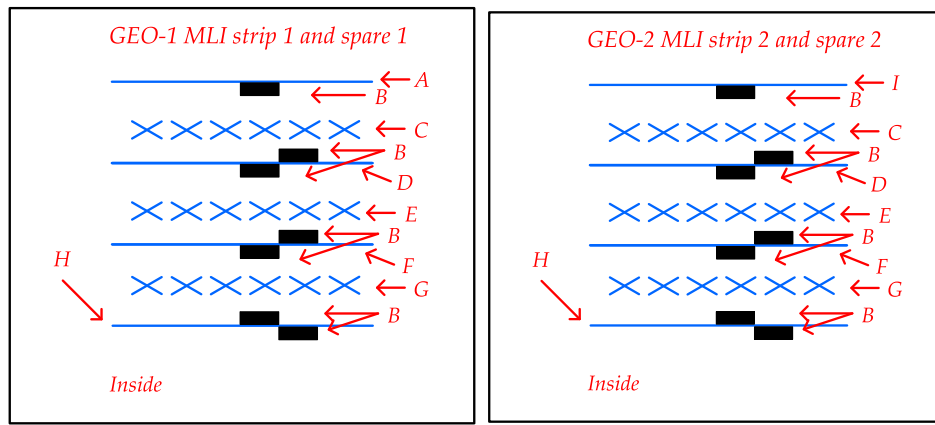
- Sample holder

The MLI and painting samples as mounted on sample plate are shown in Fig. 6.

In Fig. 6 (A) are the PT100 wires; (B) are the clip/washers; (C) are the Velcros/staples; (D) is the MLI2; (E) is the MLI1; (F) is the PSB/CFRP; (G) is the PNC/Au4G; (H) is the PSB/Au4G; (I) is the SG121FD/Au4G; (J) is the ground connection. In Fig. 6 MLI layouts strips size is 44 mm × 120 mm. Paint samples size is 20 mm × 20 mm. MLI are attached loosely on the adaptor plate with the clip/washers (hanging) and maintained in contact with it with Kapton tape at the bottom edge. The lateral edges of the MLI have been left opened. The two ends are closed by staples and Kapton tape (when mounted on sample holder). The MLI strips are grounded to avoid charging effects.

Painting samples have their substrate (back side) in good thermal contact with the sample plate and pressure applied with fastener bars on front side. For avoiding mechanical stress to the coating, masking during painting allowed to leave fixation zones free of coating.

The sample holder is heated through a resistor and cooled down with LN₂.



(a) (b)

Fig. 5. MLI application, showing stand-off/clipwasher.

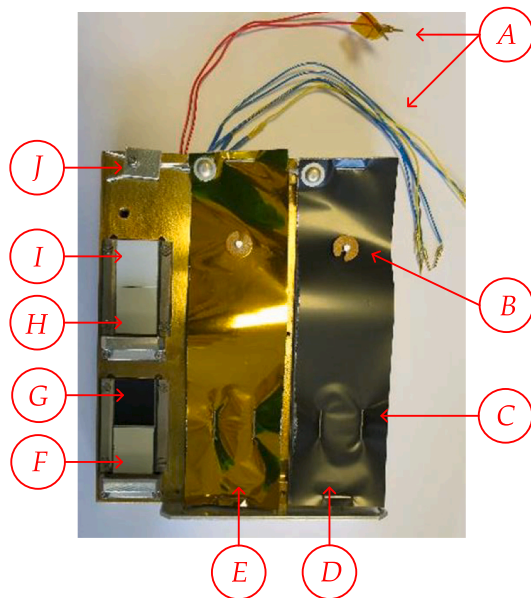


Fig. 6. GEO paint samples test flow.

Table 4 Preferred space grade paints in LEO and GEO orbits.

Samples	Paint Name	Substrate
1	SG121FD (silicone white paint)	Au4G
2	PSB (silicate white paint)	Au4G
3	PSB (silicate white paint)	CFRP
4	PNC (silicone black)	Au4G

3.2. Experimental procedures on test preparation

• Contamination

Precautions (overall cleanliness of facilities, bake-out of sample plate) were taken to avoid and monitor contamination (intrinsic contamination or from porous samples and degradation products). A crystal quartz microbalance was also used during the test campaign. Only 20 Hz of difference were measured in situ, which is within the noise-signal margin and thus shows the absence of contamination.

• Samples handling and storage

The presence of dust on sample surface and damage due to physical contact with the sample is very critical here. Therefore, special precaution has been taken, namely: handling of samples with gloves and adequate tools to avoid damaging the samples (handling being limited to the minimum); storage at room temperature under nitrogen; use of polyethylene or polypropylene bags for protection.

• Temperature calibration prior to test campaign

Calibration of sample/holder temperature prior to the test campaign was performed. The objective was: to validate parameters set for heating/cooling rates and dwell times; to measure MLI external foil temperature under UV exposure (during electrons/protons irradiations, the power brought by the exposure is typically few mW/cm² whereas UV brought up to 100 mW/cm²).

Spare samples used for this calibration step were fitted with temperature sensors, to monitor the sample plate and MLI foils temperatures. Painting temperature is equal to sample plate temperature due to the good thermal contact ensured by the mounting principle. The temperatures measured are presented in Table 5.

Samples are irradiated with 6 suns UV resulting in a heating of the outer layer to approximately 100 °C (measured temperature). Temperature was measured with a PT100 (uncertainty of temperature of this sensor typically in the 0.1 °C to 1 °C range).

The test configuration of layers considered for the calculations is shown in Fig. 7.

In Fig. 7 (A) is 1 × 1 mm of Kapton; (B) is VDA coating; (C) is 5 × Dacron spacer plate; (D) is 5 × 0.3 mm Kapton perf.; (E) is 5 × Polyester Fleece Spacer PV-8g; (F) is 5 × 0.25 mm Mylar perf.; (G) is 1 × Polyester Fleece Spacer PV-8g; (H) is 1 × 1 mm Mylar foils Δt (t > 70) = 36 °C; (I) is stand-off/clip-washer; (J) is Kapton tape; (K) is –85 °C to +100 °C TC with 4 h periods; (L) is Velcros Δt (t > 50) = 54 °C; (M) is ≈ 100 °C at T0 (alpha = 0.35).

Table 5 MLI surface temperature under UV irradiation.

Irradiation	MLI 1 (Kapton) (°C)	MLI 2 (black Kapton) (°C)	Plate (°C) Set to
UV (6 suns)	98	92	25
	102	94	100

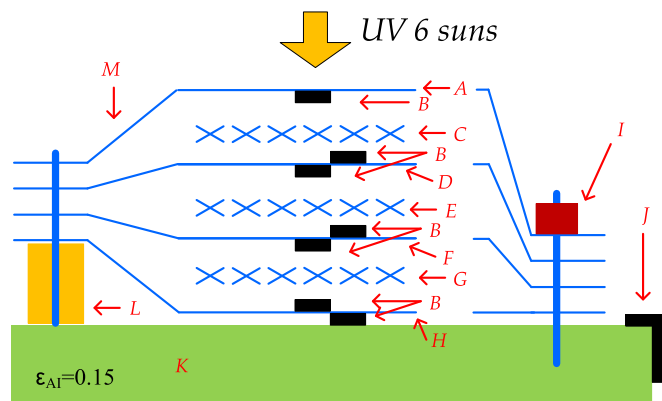


Fig. 7. Test configuration of layers considered for the calibration.

3.3. GEO test specifications

Considering a 20-year GEO mission, beams fluences are 2×10^{16} with 400 keV electrons/cm², 4×10^{15} with 240 keV protons/cm², and 4×10^{16} with 45 keV protons/cm², leading to an overall 3 week–4 week exposure with ionizing particles. The execution of the irradiations and the test sequences with details of beam currents, particle fluences and homogeneity factors (standard deviation/mean fluence) are shown in Fig. 8.

During the testing, 2 failures happened:

- 1) Failure of the Minco heater at the early stage of the testing changed for a thermo-coax device considered as more reliable. The mending step required a venting/pumping step that could not affect the final results as failure happened very early in the test campaign (520 ESH, i.e. equivalent sun hours).
- 2) Temperature regulation failure: the electronics in charge of thermal regulation (TC program with defined parameters) failed probably due to dose effect (electron irradiation produces secondary X-rays in

the room). The failed board was changed and the automatic system shielding against secondary radiation improved.

During the failure, the samples' temperature returned to positive level (~60 °C in absence of UV) during about 72 h (failure at week-end). This failure too could not affect final results (no overheating of samples, short duration compared to total duration of testing).

3.4. GEO samples test flow

The GEO MLI/paint samples test flow is shown in Fig. 9.

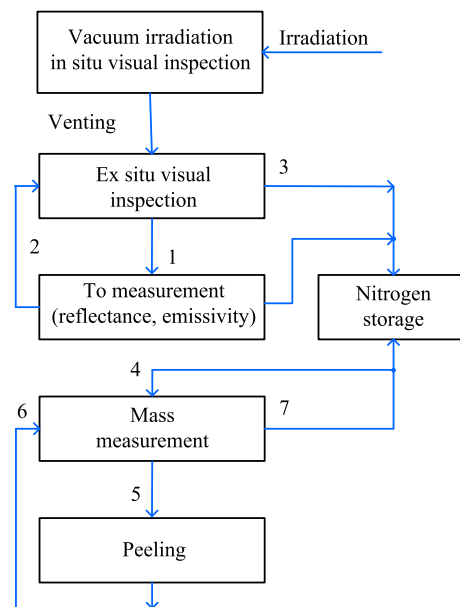


Fig. 9. GEO MLI/paint samples test flow.

	Transition					5 years			10 years	
	Air	Vacuum							p	
		23/10	26-oct			03-nov			chgt	
comment									13-nov	
TC (#cycles)				replacement with thermo-coax heater failure				60		100
UV (ESH)			520				1613		---	3000
Electrons 400keV										
2E16					15nA				17.4nA	
					5E15				5E15	
Protons 240keV										
4E15						21.5nA			24nA	
						2E15			2E15	
						19.4%			21%	
Protons 45keV										
4E16							23.4nA		27.2nA	
							1E16		1E16	
							15%		10%	
visual inspection		X	X		X	X		X		X

			12 years		14 years		16 years		18 years		20 years	Transition
					lamp							Vacuum/Air
					chgt							
							2-dec				11-dec	21-dec
comment			replacement of regulation circuit failure 3 days									
TC (#cycles)			186		200						255	300
UV ESH			4300		5445						6684	8211
Electrons 400keV												
2E16			18.2nA		17.4nA		17.7nA		18.8nA		20.4nA	
			2E15		2E15		2E15		2E15		2E15	
Protons 240keV												
4E15												
Protons 45keV												
4E16												
			24.6nA		25nA		25.7nA		25.8nA		20nA	
			5E15		5E15		5E15		5E15		5E15	
			12.5%		12%		17%		13%		16.6%	
visual inspection			X		X		X		X		X	X

Fig. 8. Test sequence with each beam current (defines flux: 1 nA/cm² = 6.4 × 10⁹ part./cm².s), deposited fluence and homogeneity (for protons; with electrons homogeneity is ±10%).

In Fig. 9 the text box “In situ visual inspection” addresses the initial paintings and MLI inspection and evolution of thermo-optical properties, which is included inspection of any self-flaking, discolouration of white paints and photos; the text box “Ex situ visual inspection” addresses ex situ visual and mechanical properties inspection, which includes visual and mechanical properties inspection after dismantling from sample plate, provides the same outputs as in situ ones; the text box “Mass measurement” addresses the measuring the mass loss of paintings and MLI; the text box “Peeling” addresses the peeling test to evaluate the mass loss of paintings and MLI. Final sample characterization is the final inspection of the material sample for evaluation by photos and mass determination.

4. Experimental results

4.1. In situ visual inspection and evolution of thermo-optical properties

In situ observation of painting did not reveal any self-flaking, but discolouration of white paints mostly. Fig. 10 discloses pictures showing evolution of yellowing/browning of the white paints and the very slight whitening of the black one (20-year picture). This discolouration effect is due to the shift of the reflectance cut-off in the UV part of the spectrum (modification of chemical structure induced by radiation: scission/cross-linking of chains in binder, coloured centres in pigments) leading to increased solar absorptance. The Evolution of solar absorptance in the range from 250 nm to 2500 nm is presented in Table 6.

Table 6

Evolution of solar absorptance in the range values 250 nm–2500 nm.

Sub-system	Initial	20 year Geo	Delta	Delta (%)
SG121FD/Au4G	0.233	0.626	0.393	169
PSB/CFRP	0.142	0.659	0.517	365
PSB	0.131	0.623	0.491	374
PNC	0.973	0.967	-0.006	-1
Black MLI	0.930	0.880	-0.050	-5
MLI	0.350	0.680	0.330	94

End-of-Life alpha are consistent with existing data (orders of magnitude) for lower but equivalent dose levels [36,37].

The first consequence of solar absorptance increase is the potential overheating of MLI external foil during the test campaign (evolution of thermal conditions of the assembly).

Table 7

Evolution of emissivity in the range values 3 μm–21 μm.

Sub-system	Initial	20 year Geo	Delta	Delta (%)
SG121FD/Au4G	0.895	0.868	-0.027	-3.0
PSB/CFRP	0.886	0.897	0.011	1.2
PSB/Au4G	0.895	0.902	0.007	0.8
PNC	0.906	0.901	-0.005	-0.6
Black MLI	0.839	0.798	0.041	4.9
MLI	0.660	0.677	-0.017	-2.6














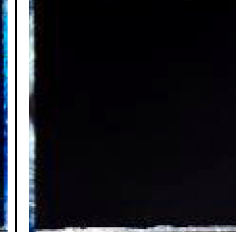
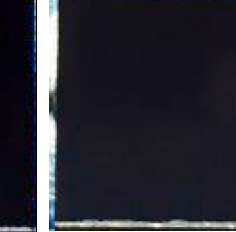
Paint	Initial	5 years	10 years	20 years	comments
PSB/Al					Homogeneous colouration No self-flaking
PSB (on CFRP)					Homogeneous colouration No self-flaking (except edge due to adherence issue on CFRP) Paint run observed
SG121FD					Homogeneous colouration No self-flaking
PNC					Very slight whitening No self-flaking

Fig. 10. Visual inspection (i.e. photos during irradiation).

The emissivity, known to be less sensitive, has also been measured, and is presented in Table 7.

Paint photos during irradiation is shown in Fig. 10.

The reflectance curves of the paintings (% vs wavelength) is shown in Fig. 11.

4.2. Ex situ visual inspection and mechanical properties

The sequence for testing is the following:

- 1) Visual inspection of samples (pre-peeling, after TO measurements);
- 2) Mass measurement;
- 3) Peeling: 3.1) Compress tape onto sample with load of nominal 5 kg for 60 s; 3.2) pull apart tape and sample at a nominal 0.2 cm/min until separation happens;
- 4) Mass measurement;
- 5) Visual inspection of samples and tapes (post peeling).

Ex situ visual inspection (after dismounting from sample plate) provides the same outputs as in situ ones. The ex situ pictures of the paintings before (right), after 20-year GEO (left) are shown in Fig. 12. (exposed to 20 Years) (paints before test).

Peeling test has been performed to investigate adherence of coatings

and check for degradation of peel and pull-off strength. The test was performed with PSA (pressure sensitive adhesive) tape.

There was no delamination on the SG121 samples and PNC samples.

The PSB paints sample and tapes before/after peeling are shown in Fig. 13 and Fig. 14.

For the PSB paint on aluminium, there was no sample fracture, but detachment of particles (pristine and aged) was observed. A slight enhancement of particle detachment in the central part of the aged sample was observed.

Fig. 14 shows the PSB on CFRP sample and tapes before/after peeling.

For the PSB/CFRP coating, substrate fracture in the central part (more strength) on both pristine and aged samples was observed. A larger fracture size is observed on pristine sample due to better adherence of coating surface (compared to aged sample where degradation occurred). Fracture comes from detachment of upper layers of CFRP substrate due to the bending of the sample at pulling step (“flexible” 0.5 mm substrate attached on opposite edges). Also, detachment of small parts was observed due to handling for dismounting from sample plate or TO measurements, illustrating brittleness of surface.

For the PNC samples, it was observed that peeling and pull-off strength remains good, and no flaking is observed, only particles detachment. However, the surface of painted samples turns “glassy” and

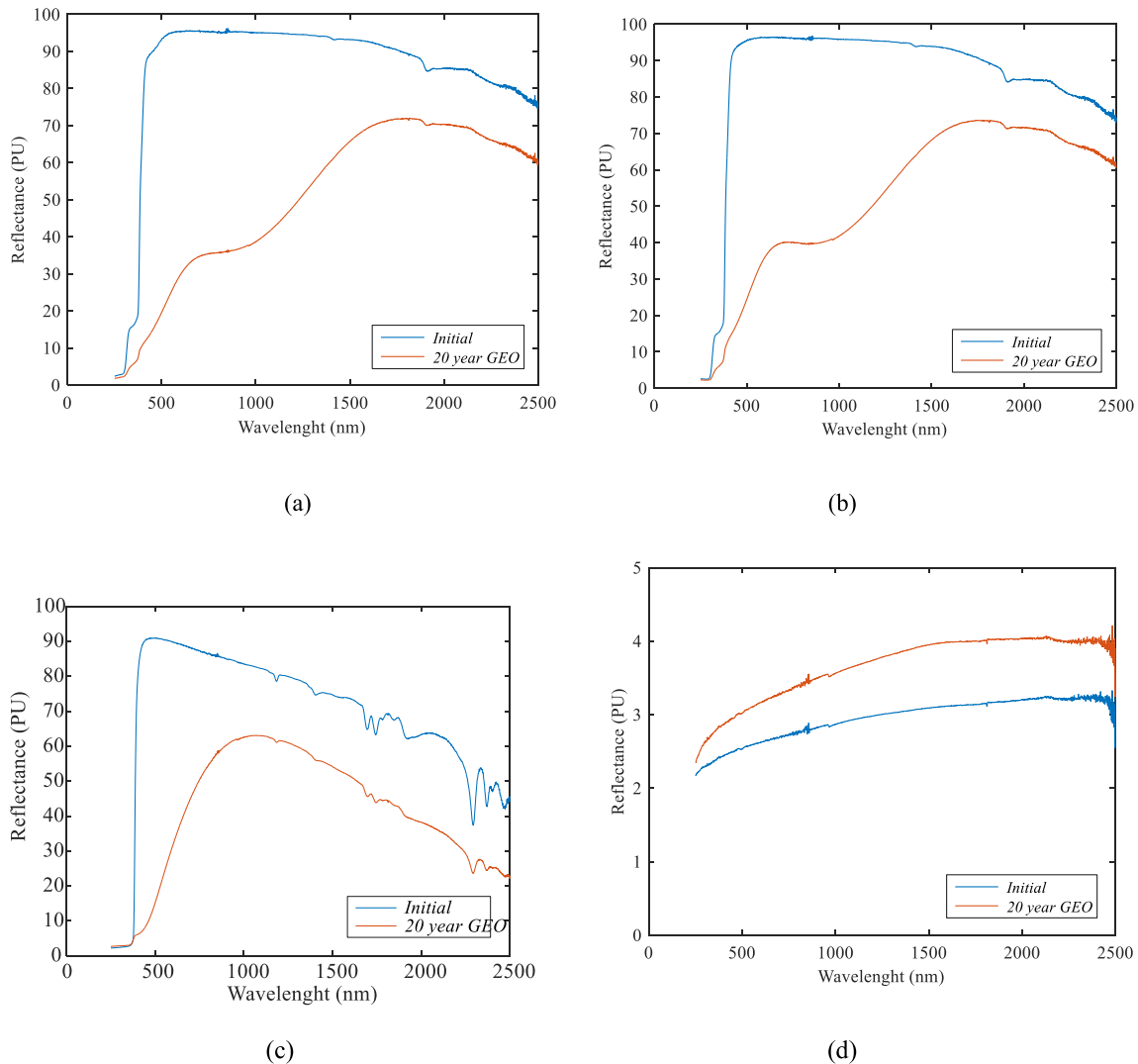


Fig. 11. Reflectance curves of the paintings (% vs wavelength). (a) and (b) exhibit the same feature (same paint, PSB, different substrates); in (d) evolution of black silicone paint PNC is very limited (see Y scale).

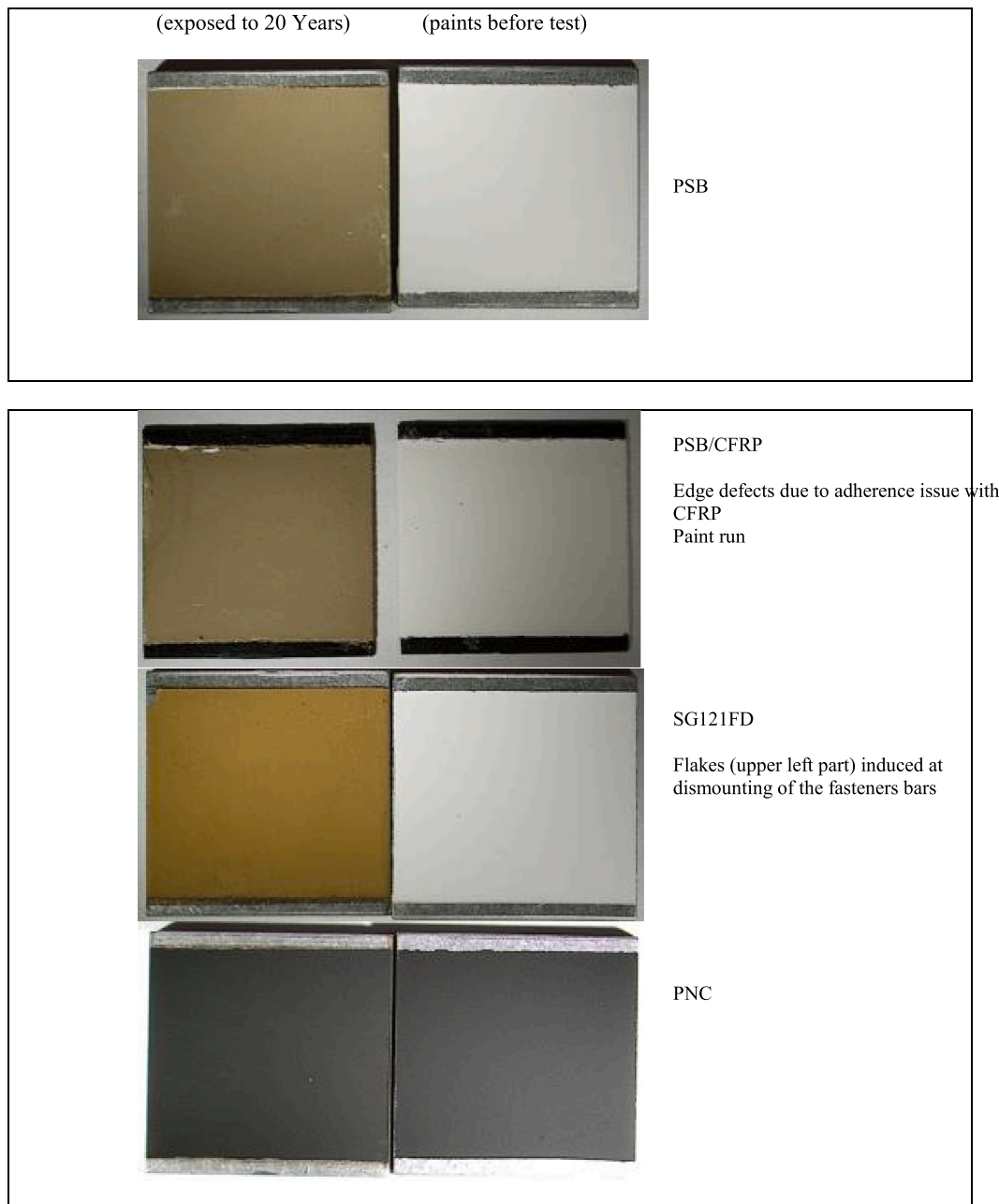


Fig. 12. Ex situ pictures of the paintings before (right) and after (left, before TO measurements) 20-year GEO.

more brittle (Proton/UV irradiation induced surface degradation).

4.3. MLI test results

In situ visual inspection did not reveal any cracks or tear initiation of external foil, but strong discolouration of Kapton (strip1), clips/washers and curling of assemblies at edges (not close). There was no visible damage of Kapton tape used to close upper/lower ends. Fig. 15.

The curled edges of the MLI (not closed) due to thermal/radiation effects are shown in Fig. 16.

From ex situ visual inspection, it appeared that Mylar (internal layers) foils of MLI assemblies were so embrittled that they fell into pieces at handling. It was therefore decided to cut one edge of the strip to allow for flipping the assembly and take pictures foil by foil.

Then, each Mylar foil has been removed, piece by piece, and “re-assembled” for pictures. Procedure for dismantling MLI for adaptor plate is shown in Fig. 17.

Figs. 18–22 shows all foils from strip 1 (see Fig. 21). It results that:

- Mylar foils are brittle (especially around Velcros);
- Polyester fleece is yellowed but not brittle;
- Kapton inner foils are not brittle;
- Dacron spacers are yellowed but not brittle;
- Kapton external foil is discoloured and not brittle;
- Velcros are bended, brittle and discoloured;
- Clip/washers are discoloured (darkening);
- Kapton tape used to close top/bottom strip ends is discoloured but not brittle.

The ex situ visual inspection of the Velcros revealed bending features, darkening and brittleness.

Bending can be due to combined temperature/dose effects. The vitreous transition temperature T_v of Nylon is quite low (in the 47 °C-60 °C range). When temperature is greater than T_v (probably in the duration of

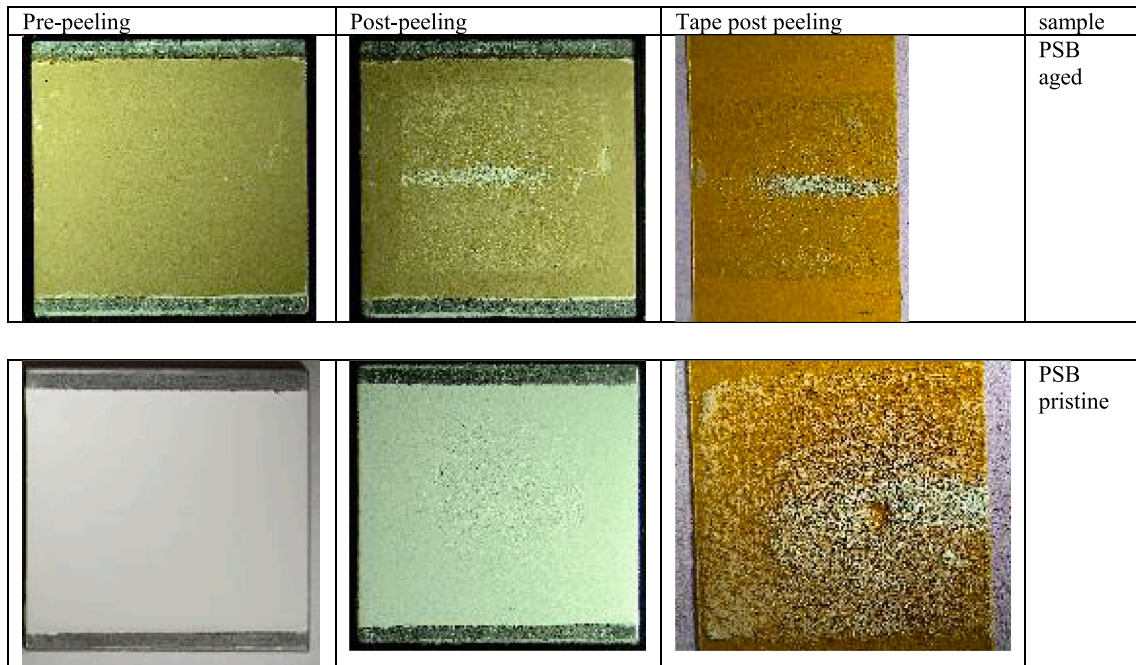


Fig. 13. PSB on aluminium Samples and tapes before/after peeling.

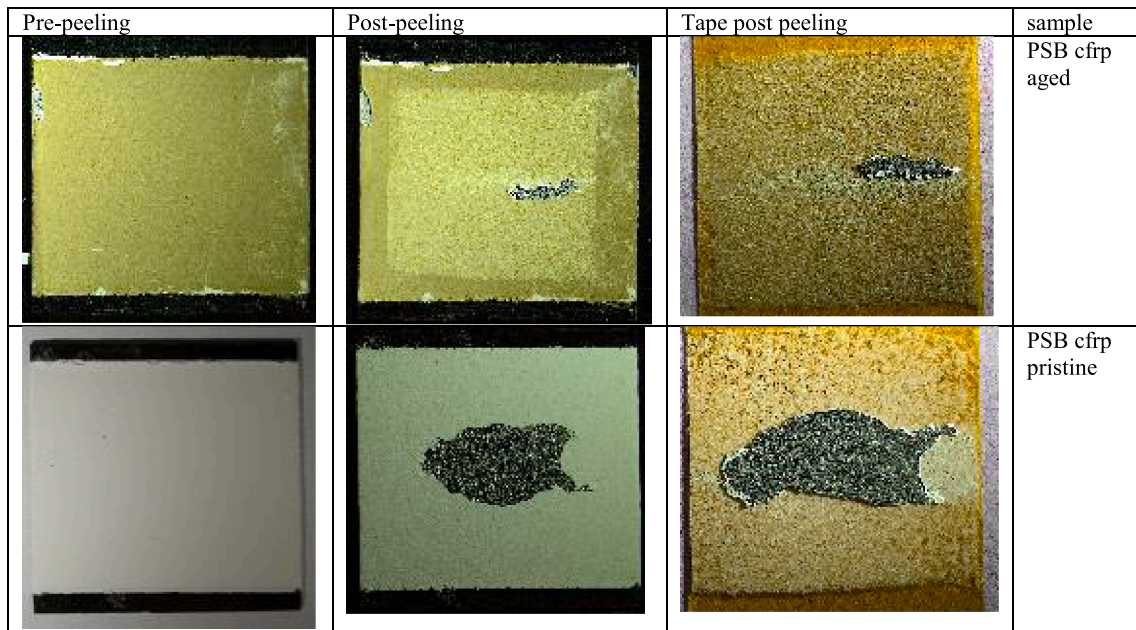


Fig. 14. PSB on CFRP Sample and tapes before/after peeling.

the cycle above +35 °C, see section 2.4), polymer chains are more mobile and sensitive to dose-induced scission, then cross-linking leading to hardened and more brittle material. This effect also occurs at loops level.

Bending also induces local mechanical stress of attached foils, and then as Mylar is also strongly degraded a “cutting at edges” mechanism takes place (at handling).

Regarding thermo-optical properties of external foils, the shift of the cut-off of the reflectance curve for strip 1 is characteristic of darkening of Kapton (more absorption in the 500 nm–1000 nm range is shown in Fig. 23b).

Regarding the black MLI, the whole spectrum is affected with higher reflectance which is characteristics of whitening of the black Kapton is shown in Fig. 23a.

4.4. MLIs: debris distributions

ImageJ, a public-domain image processing program, was used to extract debris area distribution from the set of pictures provided in section 4.3.

Fig. 24 discloses all distributions by layer for Kapton and Black Kapton MLI assemblies with “bins start” in mm² (debris area) and with Layer 1 the “back layer” (in contact to the sample holder).

As a reminder, this debris has been generated from handling and not from self-delamination or self-flaking (even if layer 1 from strip 1 was almost self-flaking). An uncertainty of 10%–20% is estimated on area measurements, as the debris could not be flattened between transparent plates due to high electrostatic conditions. The debris distribution by

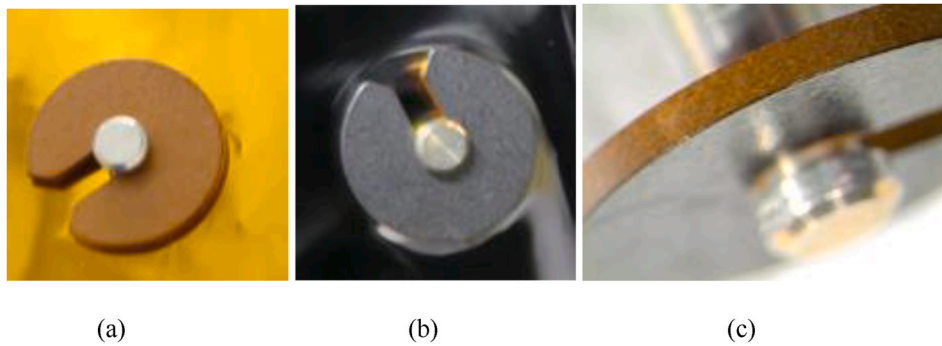


Fig. 15. Clip/washer pictures before/after GEO test campaign (in and ex situ): (a) Initial feature; (b) 20-year GEO Shadowing of MLI ext. layer underneath; (c) greater degradation at surface (p+).

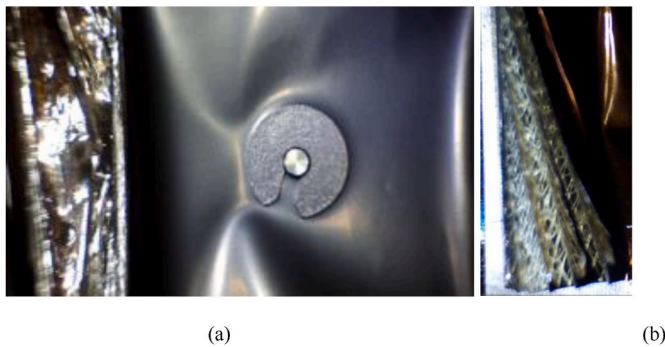


Fig. 16. Curled edges of the MLI (not closed) due to thermal/radiation effects.

layer is disclosed in Fig. 24.

5. Conclusions

Satellite material testing is usually done for the satellite expected lifetime. However defunct satellites in GEO are exposed to very long periods, beyond satellite lifetime. In this paper we study the effects of synergistic effects of space environment (electrons, VUV, protons, TC) on materials for long periods. The aim was to evaluate the creation of debris by degradation of the materials.

The materials studied were representative spacecraft GEO materials, namely: two MLI blanket samples (GEO-1 MLI layup and GEO-2 MLI) fixed to the sample holder with Nylon6.6 Velcros and Vestel standoffs and four paints SG121FD (silicone white paint) on Au4G, PSB (silicate

white paint) on Au4G, PSB (silicate white paint) on CFRP, PNC (silicone black) on Au4G.

A simulation of 20-year of GEO dose profile was performed combining particles and UV doses in synergy with thermal cycling. Beams fluences were: 2×10^{16} with 400 keV electrons/cm², 4×10^{15} with 240 keV protons/cm², and 4×10^{16} with 45 keV protons/cm². The TC was 300 cycles, from -85 °C to $+100$ °C. UV simulation was provided with Xenon 6500 lamp whose spectrum is close to the solar spectrum, the sun acceleration was measured periodically and adjusted between 5.2 and 6.6SC (variation due to lamp ageing) a total of 8211 ESH was done.

As to major results, in situ observation of painting did not reveal any self-flaking, but discolouration of white paints was observed. The discolouration of white paints showed an evolution to yellowing/browning. The evolution of solar absorptance in the paints and MLI external foil was measured. The major degradation was observed in SG121FD on Au4G (absorptance changed from 0.233 to 0.626), PSB on CFRP (absorptance changed from 0.142 to 0.659), PSB (absorptance changed from 0.131 to 0.623) and MLI (absorptance changed from 0.350 to 0.680). The first consequence of solar absorptance increase is the potential overheating of MLI external foil during the test campaign (evolution of thermal conditions of the assembly). Emissivity was also measured but changes were less relevant.

Adhesion test on paints have not indicate major differences in paint adhesion of the aged samples compared with the reference samples.

Regarding debris generation by material aging due to space environment, the more relevant results were obtained from MLI degradation. The external layers of the MLI layups were curled and TO properties changed significantly (i.e. burned up appearance). After disassembling the MLI layups it was found that the Mylar inner foils were brittle and

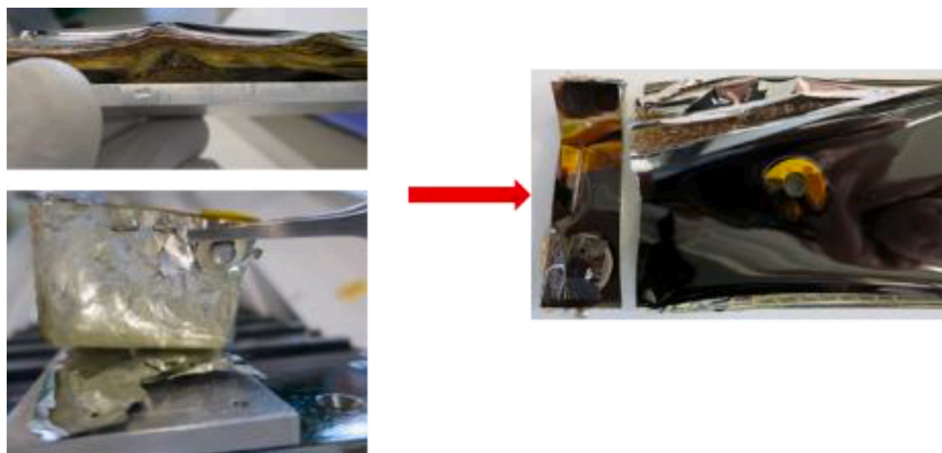


Fig. 17. Procedure for dismantling MLI for adaptor plate.

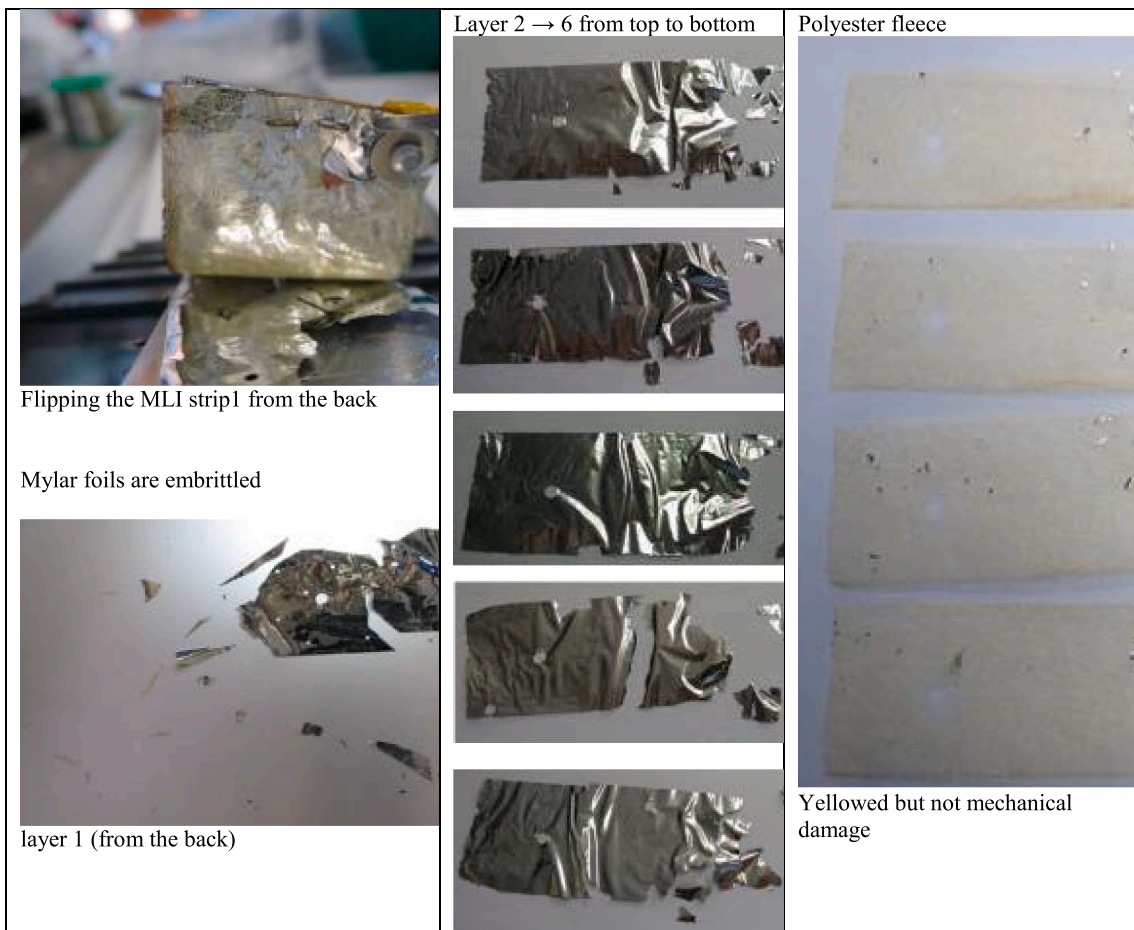


Fig. 18. Mylar foils and polyester fleeces from strip1 (numbering from the back foil).



Fig. 19. Flipping the Kapton/dacron foils of strip1 (layer 7 to 12 numbering from the back foil).

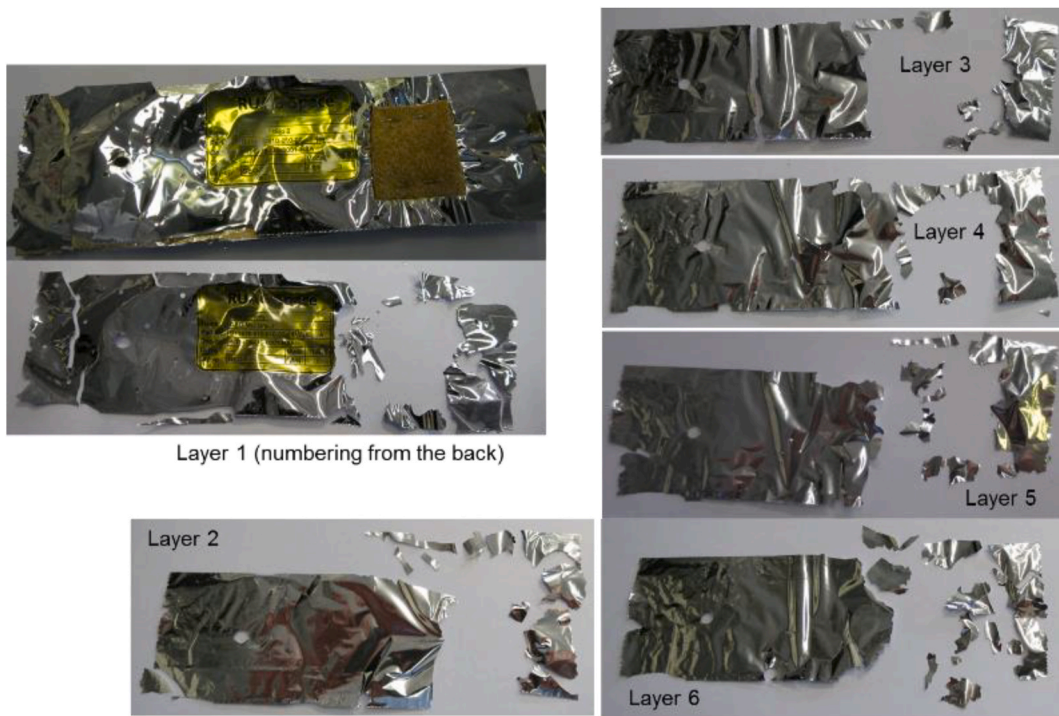
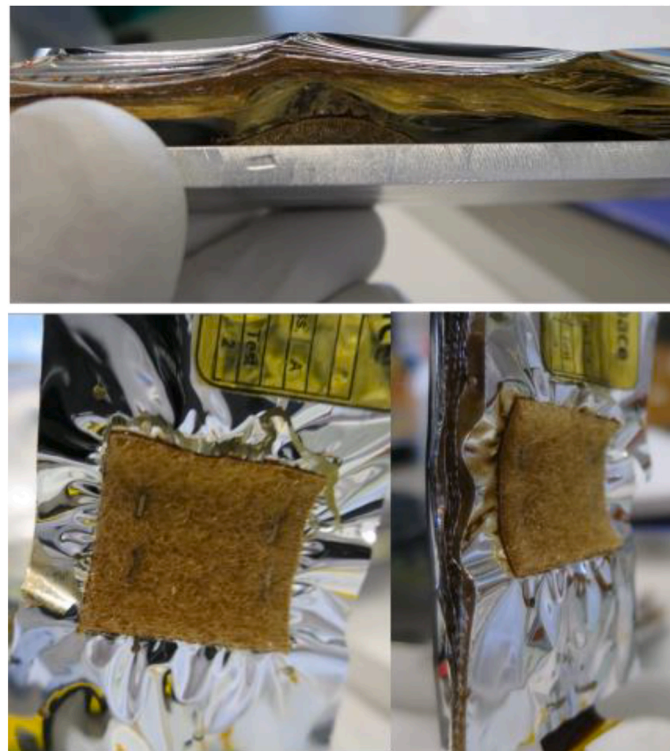


Fig. 20. Mylar foils and polyester fleeces from strip2 (numbering from the back foil).





(a)

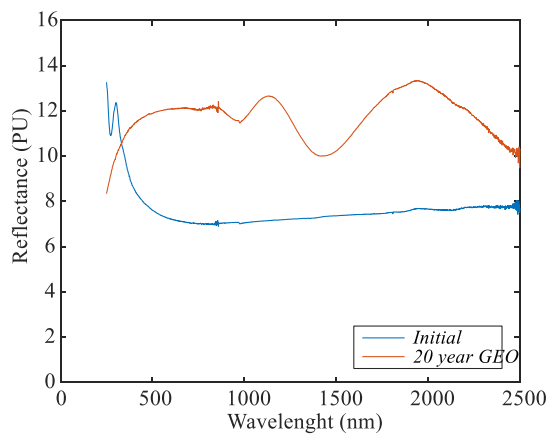


(b)

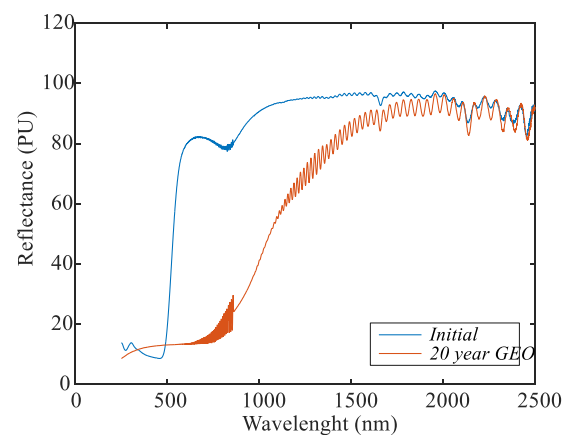
(c)

(d)

Fig. 22. Velcros degradation; (a) degradation; (b) Darkening of Velcros (loops); (c) and (d) embrittled Velcros (broken parts at handling).



(a)



(b)

Fig. 23. Reflectance curves of the MLI external layers (R% vs wavelength): (a) black Kapton (strip2), (d) Kapton (strip1).

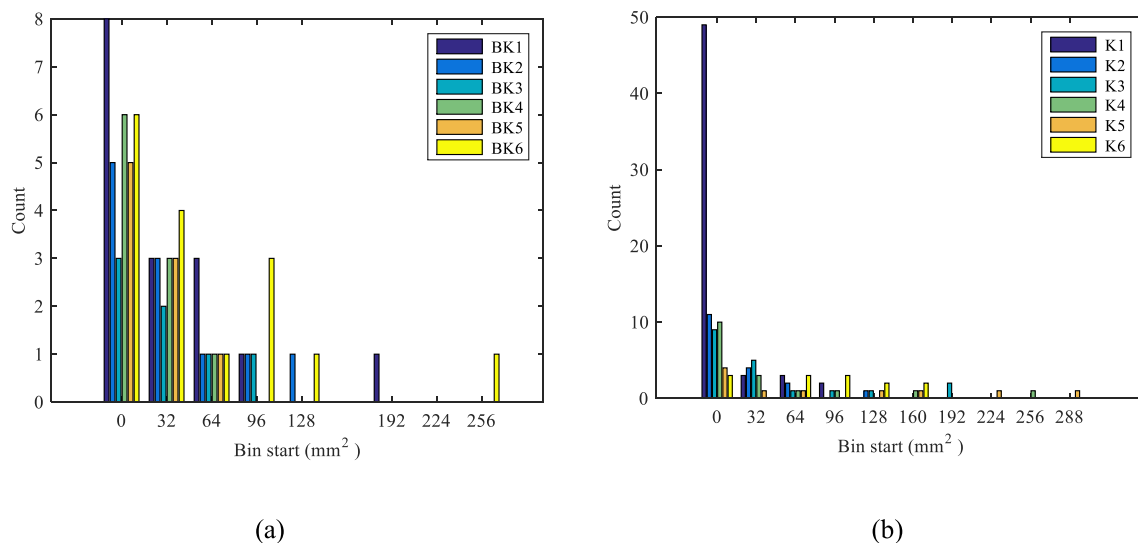


Fig. 24. Debris distributions for all layers; bins start is in mm² (debris area): (a) Kapton layout, K1 is the first layer in contact with sample holder; (b) Black Kapton layout, BK1 is the first layer in contact with sample holder; Bins start is in mm² (debris area).

fell into pieces at handling. Extreme care was taken handling the brittle MLI layers, the Debris distributions for the layer was measured.

Regarding the MLI fixation methods the Velcros degraded extremely, becoming yellow and brittle. It may be possible that severe degradation of the Velcro leads to the separation of the full MLI blanket (if the MLI is only attached with Velcros) however to prove this hypothesis further study is needed.

These results are expected to contribute to a better practice of choice of materials when building satellites, to avoid the significant problems caused by debris.

Declaration of competing interest

The authors declare that they have no known competing financial interests or personal relationships that could have appeared to influence the work reported in this paper.

Acknowledgment

This research received no external funding. The ongoing work presented in this paper was performed under ESA contract 4000113047/14/NL/LF/TU-IAS, Space Debris from Spacecraft Degradation Products; Foundation for Science and Technology (FCT), through CENTRA, project UIDB/00099/2020; Foundation for Science and Technology (FCT) under the LAETA project UIDB/50022/2020; Foundation for Science and Technology (FCT) under the ICT (Institute of Earth Sciences) project UIDB/04683/2020.

References

- [1] I. Levchenko, O. Baranov, J. Fang, O. Cherkun, S. Xu, K. Bazaka, Focusing plasma jets to achieve high current density: feasibility and opportunities for applications in debris removal and space exploration. *Aero. Sci. Technol.* 108 (2021), 106343.
- [2] L. Felicetti, R. Emami, Image-based attitude maneuvers for space debris tracking. *Aero. Sci. Technol.* 76 (2018) 58–71.
- [3] F. Cichocki, M. Merino, E. Ahedo, Spacecraft-plasma-debris interaction in an ion beam shepherd mission. *Acta Astronaut.* 146 (2018) 216–227.
- [4] V.A. Obukhov, V.A. Kirillov, V.G. Petukhov, G.A. Popov, V.V. Svitina, N.A. Testoyedov, I.V. Usovik. Problematic issues of spacecraft development for contactless removal of space debris by ion beam. *Acta Astronaut.* 181 (2021), 569–578.
- [5] T. Schildknecht, *Astron. AstroPhys. Rev.* 14 (2007) 41–111.
- [6] D.S. McKnight, F.R. Di Pentino, New insights on the orbital debris collision hazard at GEO. *Acta Astronaut.* 85 (2013) 73–82.
- [7] N.L. Johnson, A new look at the GEO and near-GEO regimes: operations, disposals, and debris. *Acta Astronaut.* 80 (2012) 82–88.
- [8] Technical Report on Space Debris, United Nations, New York, USA, 1999.
- [9] E.M. Silverman, *Space Environmental Effects on Spacecraft: LEO Materials Selection Guide*, National Aeronautics and Space Administration (NASA), Hampton, USA, 1999.
- [10] P. Gordo, T. Frederico, R. Melicio, S. Duzellier, A. Amorim, System for space materials evaluation in LEO environment, *Adv. Space Res.* 66 (2) (2020) 307–320.
- [11] P. Gordo, T. Frederico, R. Melicio, A. Amorim, Implementation of a cryogenic facility for space debris analysis, *Appl. Sci.* 11 (3) (2020) 1–25, 948.
- [12] S. Duzellier, P. Gordo, A. Horstmann, G. Drolshagen, J.F. Roussel, Degradation of MLI and painting induced generation of debris, in: *Proc. of 67th International Astronautical Congress*, 2016, pp. 1–5. Guadalajara, Mexico.
- [13] K. Mori, J. Ishizawa, Temperature effects of ultraviolet irradiation on material degradation, in: *Protection of Materials and Structures from the Space Environment*, vol. 32, Springer, Berlin, Germany, 2013, pp. 399–407.
- [14] J. Marco, S. Remaury, C. Tonon, Eight years GEO ground testing of thermal control coatings, in: *Proc. of 11th International Symposium on Materials in the Space Environment*, 2009, pp. 1–9. Toulouse, France.
- [15] R.L. Kiefer, R.A. Orwoll, *Space Environment Effects on Polymeric Materials*, National Aeronautics and Space Administration (NASA), Hampton, USA, 1987.
- [16] V.I. Pavlenko, V.I. Onishchuk, Z.V. Pavlenko, K.A. Orekhov, Effect of radiation on glasses in borosilicate and boron-lead-silicate systems, *Glass Ceram.* 59 (2002) 11–13.
- [17] M. Tavlet, S. Llie Tonon, Behaviour of organic materials in radiation environment, in: *Proc. of IEEE 5th European Conference on Radiation and its Effects on Components and Systems*, Fontevraud, France, 1999, pp. 210–215.
- [18] H. Schonbacher, B. Szeless, M. Tavlet, K. Humer, H.W. Webert, Results of Radiation Tests at Cryogenic Temperature on Some Selected Organic Materials for the LHC, *Organisation Européenne pour la Recherche Nucleaire (CERN)*, Geneva, Swiss, 1996.
- [19] L.B. Fogdall, S.S. Cannaday, Space radiation effects of a simulated Venus-Mercury flyby on solar absorptance and transmittance properties of solar cells cover glasses and adhesives, in: *Proc. of AIAA 6th 6th Thermophysics Conference*, 1971, pp. 1–12. Tullahoma, USA.
- [20] M. Moser, C.O.A. Semprinoschnig, M.R.J. Van Eesbeek, R. Pippin, Surface and bulk degradation of teflon FEP retrieved from the hubble space telescope solar arrays, *High Perform. Polym.* 20 (2008) 429–446.
- [21] J.A. Townsend, C. Powers, M. Viens, M. Ayers-Treusdell, B. Muñoz, Degradation of teflon FEP following charged particle radiation and rapid thermal cycling, in: *Proc. of NASA Conference Publication*, Hampton, USA, 1999, pp. 247–256.
- [22] B.A. Briskman, E.R. Klinshpont, V.F. Stepanov, K.B. Tlebaev, Determination of dose rate effects in polymers irradiated in vacuum, *J. Spacecraft Rockets* 41 (3) (2004) 360–365.
- [23] W.R. Hardgrove, Space simulation test for thermal control materials, in: *Proc. Of 16th Space Simulation Conference: Confirming Spaceworthiness into the Next Millennium*, vol. 3096, 1991, pp. 267–285. Washington, USA.
- [24] O. Husmann, K. Kerner, J. Naegel, The influence of the UV-intensity on IF-filter protected second surface mirror alpha sub s stabilities, including surfaces with conductive top layers (solar absorption effects), in: *Proc. of USAF/NASA International Spacecraft Contamination Conference*, Redstone Arsenal, USA, 1978, pp. 1089–1111.
- [25] S. Duzellier, C. Pons, S. Remaury, P. Nabarra, Influence of test conditions and variability of end-of-life solar absorptance of thermal control materials, in: *Proc. of 14th International Symposium on Materials in Space Environment*, Biarritz, France, 2018, pp. 1–7.
- [26] J.A. Dever, B.A. Banks, L. Yan, Vacuum ultraviolet radiation effects on DC93-500 silicone film, in: *Protection of Materials and Structures from the Space Environment*, Springer, Dordrecht, The Netherlands, 2006, pp. 123–140.

- [27] European Space Research and Technology Centre, The particle and ultraviolet (UV) radiation testing of materials, in: ESA PSS-01-706 Issue 1, Noordwijk, The Netherlands, 1983, pp. 1–36.
- [28] ASTM E512-94, Standard Practice for Combined, Simulated Space Environment Testing of Thermal Control Materials with Electromagnetic and Particulate Radiation, ASTM International, West Conshohocken, USA, 2020.
- [29] Ecsc-Q-ST-70-06C, Particle and UV Radiation Testing for Space Materials, ESA Requirements and Standards Division, Noordwijk, The Netherlands, 2008.
- [30] Y. Haruvy, Radiation durability and functional reliability of polymeric materials in space systems, *Int. J. Radiat. Appl. Instrum. C Radiat. Phys. Chem.* 35 (1–3) (1990) 204–212.
- [31] J.L. Prebola, D.H. Crider, D.S. Crews, Evaluation of enhancements to the AEDC combined space environment chamber, in: Proc. of 45th, AIAA Aerospace Sciences Meeting and Exhibit, Reno, USA, 2007, pp. 1–8.
- [32] J.A. Dever, C.R. Stidham, T.M. Dever, J.A. Terlep, Simulation of the synergistic low earth orbit effects of vacuum thermal cycling, vacuum UV radiation, and atomic oxygen, in: Proc. of 7th Space Simulation Conference, 1992, pp. 19–36. Baltimore, USA.
- [33] J.A. Dever, E.J. Bruckner, Synergetic effects of ultraviolet radiation, thermal cycling and atomic oxygen on altered and coated kapton surfaces, in: Proc. of 30th Aerospace Sciences Meeting & Exhibit, 1992, pp. 1–10. Reno, USA.
- [34] B.A. Briskman, E.R. Klinshpont, V.I. Tupikov, Space environment simulation at radiation test of nonmetallic materials, *Nucl. Instrum. Methods Phys. Res. B* 151 (1999) 427–453.
- [35] Surface Treatment Experts, Metal plating on satellites: the benefits of light reflection, available online: <https://www.sharrettsplating.com/blog/metal-plating-satellites-benefits-light-reflection/>, 2019. (Accessed 4 February 2021).
- [36] Comparaison de la tenue à l'environnement spatial des peintures silicones blanches SG120FD et SG121FD. MAP paint evaluation report: DTS/AE/MTE/TH/03-057. Falta ano (accessed 13 June 2020).
- [37] J. Marco, S. Remaury, C. Tonon, Eight years GEO ground testing of thermal control coatings, in: Proc. of International Symposium on Materials in a Space Environment, 2009, pp. 1–9. Aix-En-Provence, France.